



Mehdizadeh, A., Disfani, M. M. and Shire, T. (2021) Post-erosion mechanical response of internally unstable soil of varying size and flow regime. *Canadian Geotechnical Journal*, 58(4), pp. 531-539.

There may be differences between this version and the published version. You are advised to consult the publisher's version if you wish to cite from it.

<http://eprints.gla.ac.uk/217382/>

Deposited on: 4 June 2020

Enlighten – Research publications by members of the University of Glasgow
<http://eprints.gla.ac.uk>



Canadian Geotechnical Journal

Post-erosion mechanical response of internally unstable soil of varying size and flow regime

Journal:	<i>Canadian Geotechnical Journal</i>
Manuscript ID	cgj-2019-0790.R1
Manuscript Type:	Article
Date Submitted by the Author:	n/a
Complete List of Authors:	Mehdizadeh, Amirhassan; The University of Melbourne Disfani, Mahdi; The University of Melbourne, Infrastructure Engineering Shire, Thomas; University of Glasgow, School of Engineering
Keyword:	Internal erosion, Post-erosion behavior, Flow regime, Internal stability, Suffusion
Is the invited manuscript for consideration in a Special Issue? :	Not applicable (regular submission)

SCHOLARONE™
Manuscripts

**Post-erosion mechanical response of internally unstable soil of varying size
and flow regime**

Authors:

Amirhassan Mehdizadeh¹, Mahdi Miri Disfani² and Thomas Shire³

¹: Amirhassan Mehdizadeh, orcid.org/0000-0001-7711-8128

MSc, PhD, Research Fellow in Geotechnical Engineering, Department of Infrastructure Engineering, University of Melbourne, Melbourne, Australia, amehdizadeh@unimelb.edu.au

²: Mahdi Miri Disfani, orcid.org/0000-0002-9231-8598

MSc, PhD, Senior Lecturer in Geotechnical Engineering, Department of Infrastructure Engineering, University of Melbourne, Melbourne, Australia, mmiri@unimelb.edu.au

³: Thomas Shire, orcid.org/0000-0002-8005-5057

PhD, Lecturer in Geotechnical Engineering, James Watt School of Engineering, University of Glasgow, UK, Thomas.shire@glasgow.ac.uk

Corresponding Author:

Mahdi M. Disfani², orcid.org/0000-0002-9231-8598

MSc, PhD, Senior Lecturer in Geotechnical Engineering, Department of Infrastructure Engineering, University of Melbourne, Melbourne, Australia, mmiri@unimelb.edu.au

Keywords

Internal erosion; Post-erosion behavior; Flow regime; Internal stability; Suffusion

Abstract

One of the leading causes of dam failure is internal erosion. The impact of erosion of non-plastic fine particles, known as suffusion, on the soil structure and strength has been studied experimentally. However, influences including sample size have not been thoroughly investigated. Internally unstable gap-graded cohesionless soil samples with various sizes were investigated using an erosion-triaxial apparatus. Samples were subjected to downward inflows of different seepage velocities. The results indicated that the potential for clogging increased with an increase in specimen length, leading to less fine particle erosion. Internal erosion changed the mechanical soil behaviour even after the loss of fines equal to five percent of the overall sample volume. Eroded specimens with similar intergranular void ratios showed similar undrained post-erosion behaviour. However, the magnitude of the post-erosion initial undrained peak shear strength is a function of coarse particle interlocking, residual fine content and equivalent intergranular contact index. It was also found that the steady state line remained unchanged after erosion of fine particles and the mobilized friction angle at the steady state line is independent of the residual fine content.

Introduction

Internal erosion is one of the major causes of hydraulic structure failure (ICOLD, 2015). According to ICOLD (2015), internal erosion is divided into four main mechanisms: concentrated leaks, backward erosion, contact erosion and suffusion. The focus of this research is suffusion, the migration of non-plastic fine particles from within a matrix of coarser particles due to a seepage flow within an embankment dam or its foundation. It normally occurs in gap or broadly graded internally unstable soils where fine particles are not fully involved in stress transfer.

Among the first experimental works studying of the impact of erosion of non-plastic fine particles on the post-erosion mechanical behaviour of soils, Chang and Zhang (2012) and Chen et al. (2016) investigated the drained shear strength of eroded specimens. They found a decline in the drained shear strength and alteration of soil behaviour from dilative to contractive following erosion of fines. It was believed that an increase in the void ratio due to the removal of fine particles shifted the soil to a looser state. Post-erosion undrained behaviour of granular mixtures subjected to suffusion was studied by Xiao and Shwiyhat (2012) and Ke and Takahashi (2014). It was found that the undrained shear strength increased after erosion of the fine particles. Xiao and Shwiyhat (2012) stated that this might have occurred due to a loss of saturation during the erosion stage. However, Ke and Takahashi (2014) believed that the higher undrained strength of the eroded specimen may have been attributed to formation of local reinforcement in the soil fabric due to particle rearrangement. Post-erosion drained behaviour of the same soil mixture was also studied by Ke and Takahashi (2015). Results indicated that depending on the initial fine content, the post-erosion drained shear strength may stay unchanged or decrease.

Despite these attempts to explain the post-erosion mechanical behaviour of internally unstable soils, no specific conclusion can be drawn on the impact of erosion on soil mechanical behaviour. Moreover, it appears that the impact of specimen size on the erosion of fine particles and post-erosion mechanical behaviour has been overlooked. From the few available studies on different types of internal erosion (e.g. Sellmeijer, 1988; Li, 2008; Seghir et al., 2014; Zhong et al., 2019), it is evident that the critical hydraulic gradients or hydraulic conductivity may be affected by dimensions of soil specimens although the exact impact was unclear. For instance, while Seghir et al. (2014) believed that internal erosion was independent of specimen length, Sellmeijer (1988) and Li (2008) suggested that the required hydraulic gradient for initiation of erosion had an inverse relation with the seepage length. More recently, Zhong et al. (2019) showed the critical hydraulic gradient decreases with the size of the specimen increasing.

This paper discusses results of a series of undrained triaxial tests on eroded specimens with different dimensions subjected to downward seepage inflows while comparisons are made with undrained behaviour of non-eroded specimens.

Testing Program

Gap-graded soil specimens with an initial fine content (FC_i) of 25 per cent were prepared to investigate the impact of fine particle removal on the post-erosion behaviour of an internally unstable soil. An initial fine content of 25 per cent was chosen as it is believed that contribution of fine particles in the soil stress matrix is uncertain when the fine content is in the density-dependent transitional zone (i.e. between 25 and 35 per cent), with fines being active, semi-active or inactive (Shire et al., 2014). The particle size distribution and physical properties of the soil mixture are shown in **Fig. 1** and **Table 1**. The mineralogy of particles is predominantly

quartz and Mehdizadeh et al. (2017a) showed that angularity of particles in coarse fraction is higher than that of fine fraction which may enhance the erosion resistance as stated by Marot et al. (2012). On the other hand, erosion of the more rounded fines will lead to an overall increase in the average angularity of particles and therefore an increase in post-erosion interlocking. The internal instability of this gradation was examined based on methods developed by Kezdi (1969), Kenney and Lau (1986), Burenkova (1993) and Indraratna et al. (2011) showing that the soil mixture is internally unstable.

<<Insert **Fig 1** about here>>

<<Insert **Table 1** about here>>

The soil specimens with diameters of 50, 75 and 100 mm were compacted layer by layer using the moist tamping technique (Mehdizadeh et al, 2017a), adjusting the thickness of soil layers to ensure that the soil layers in samples with different height still receive almost the same compaction energy. To achieve a high level of saturation, carbon dioxide was injected at the bottom of the specimen using a flow controller at the low rate of 1 L/min for two hours while the cell pressure was maintained constant. The cell and back-pressure were gradually increased at a rate of 1 kPa/min to 400 and 390 kPa respectively to reach the fully saturated (B-value of 0.91). All specimens were consolidated to 150 kPa after full saturation to remove the footprint of sample preparation (Frost and Park, 2003) and then a downward seepage flow was applied to the top of the specimen for two hours. The eroded soil mass was collected in a collection tank, allowing the fines content to be calculated throughout the test. The collection system was designed to collect and measure the eroded particles continuously and also to record their weights, to discharge water from the triaxial chamber and to keep the bottom of the sample

129 saturated. The collection tank was a double wall tank with a measuring container submerged
130 under a stable water level inside a cell (inner cell) and connected to a submersible load cell
131 (with 10g resolution). The water level at the top of this cell was kept constant by discharging
132 the water from the inner cell into the main chamber via drainage holes in the wall of the inner
133 cell. The air above the water was pressurized to the back-pressure applied to the specimen
134 during the test. Details of the modified apparatus, testing procedure and repeatability of tests
135 result were discussed thoroughly by Mehdizadeh et al. (2017a). Testing was performed in four
136 stages as shown in **Table 2**. It is currently a matter of discussion as to whether seepage velocity
137 or hydraulic gradient should be used to predict the onset of suffusion (Vogt et al., 2015).
138 Richards and Reddy (2008) believed that assuming Darcy's law is applicable during the
139 seepage, an increase in hydraulic gradient leads to a decrease in hydraulic conductivity at a
140 constant flow. Considering this effect, they suggested considering only critical hydraulic
141 gradient for cohesionless soils may not be correct. Ke and Takahashi, (2014) stated that there
142 is no method to accurately control and measure the head loss in tubes, valves and fittings during
143 a laboratory erosion testing which is necessary if constant hydraulic gradient method is
144 employed. Sibille et al. (2015) took both seepage velocity and hydraulic gradient into account
145 to characterize the hydraulic load by computing the power expended by the seepage flow. The
146 great influence of hydraulic loading path on the suffusion development was reported by
147 Rochim et al (2017). Considering these limitations, it was decided to keep the seepage velocity
148 constant instead of maintaining the hydraulic gradient during the erosion phase. Here, a flow
149 controller was used to maintain a constant seepage velocity in preference to a constant
150 hydraulic gradient. The inflow increased gradually to the designated velocity and then was kept
151 constant for two hours (Fig. 2).

The initial hydraulic conductivity of the soil samples was around 0.075 cm/s based on the equation proposed by Carrier (2003) which is in the range of coarse sand as expected. Three seepage velocities of 0.086 cm/s (52 mm/min), 0.153 cm/s (92 mm/min) and 0.347 cm/s (208 mm/min) were applied to the top of the samples via a perforated top cap filled with glass beads to ensure that the flow was applied as uniformly as possible. Flow velocities and applied hydraulic gradients (Table 2) were comparable with previous studies (Marot et al., 2010; Chang and Zhang, 2012; Ke and Takahashi, 2015).

<<Insert **Table 2** about here>>

<<Insert **Fig 2** about here>>

Tests result and Discussion

Impact of Erosion on the Fine Content

According to Kenney et al., (1985) and Indraratna et al., (2007), the controlling constriction size of the tested mixture in this study is in the range 0.28 to 0.3 mm. This means that the largest fine particles (in range of 0.075 - 0.3 mm) should just be able to move through the sample under seepage forces. The normalized residual fine content (FC_c/FC_i , where FC_c is the current residual fine content and FC_i is the initial fine content) with time for test series one to three is shown in **Fig. 3**. For the first series of tests, three specimens with diameters of 50, 75 and 100 mm were prepared and subjected to a seepage velocity of 52 mm/min for 120 minutes. As each erosion test progressed, it was noted that the rate of erosion for all three specimens decreased, and erosion was seen to stop by the end of the test. The rate of erosion and maximum

percentage of the eroded particles were similar for the 75 and 100 mm diameter specimens (~45% of fines eroded). However, the 50 mm diameter specimen showed significantly larger erosion (66%) despite having similar sample preparation and test procedures, suggesting that the difference is not due to soil fabric. Two possible reasons for the difference are suggested. The first scenario is attributed to the higher possibility of clogging inside the larger specimens. Following work by Kenney et al. (1985) that in a soil containing a range of constriction sizes, the chance of a fine particle encountering a smaller constriction increases with the length of a flow path. **Fig. 4** shows the effective Constriction Size Distribution (CSD) at different heights in the sample according to the method suggested by Kenney et al (1985) with the CSD calculated according to Locke et al. (2001). An assumption of D_{50} as the layer spacing is used, as suggested by Wu et al., 2012 and Taylor et al., 2019 (D_{50} is the particle diameter in which 50 per cent by weight of coarser particles passed). It is evident from **Fig. 4** that as sample length increases the effective CSD becomes finer which increases the chance of clogging. This is in agreement with the finding in this research that a higher proportion of particles was eroded from smaller samples. **Fig. 4** also shows that there is not much difference in CSD for fine particles 115.6 mm and 198.9 mm away from the base (exit point). This confirms the experimental observation that erosion of fine particles in larger samples were similar in terms of trend and magnitude. The second reason is related to inadequate seepage forces to carry the eroded particles along the larger specimens, which can lead to particle sedimentation in the downstream before washing particles out completely. However, clogging is believed to be the dominant cause.

<<Insert **Fig 3** about here>>

<<Insert **Fig 4** about here>>

In the second test series, a 75 mm diameter specimen (E-D75-V92-T120) was eroded under a higher seepage velocity (92 mm/min) for two hours (Mehdizadeh et al., 2017b). The residual fine content (FC_f) of 10.1 per cent was very close to the residual fine content of the 50 mm diameter specimen E-D50-V52-T120 in the first series of testing. The specimen with a larger diameter but higher seepage velocity (E-D75-V92-T120) initially had a lower rate of erosion, but this increased after around 15 minutes. Both specimens showed similar trends 30 minutes after the seepage initiation until the end of the erosion phase. This meant that initial clogging was more severe inside the larger specimen but after a delay, the higher seepage force allowed this to be overcome. This is interesting as theoretically it is expected to get more eroded particles under a higher seepage velocity when other influential factors such as fabric, initial condition and sample preparation are kept the same.

In the third test series, the maximum applicable seepage velocity of 208 mm/min was applied to the 50 mm diameter specimen for 120 minutes to erode the maximum possible proportion of fine particles, leading to 6.9 per cent residual fine content. Fig. 3 shows that regardless of the specimen dimensions and seepage velocity, the rate of erosion of fine particles greatly reduced despite the fact that the residual fine contents were different, and it can therefore be assumed that the majority of the inactive and semi-active particles were removed.

It is believed that inactive fine particles (sitting loose in the voids with minor participation in the force chains) are the most vulnerable to suffusion. A percentage of these free particles are washed out of the specimen, while a number of them are clogged inside the specimen. By an increase in the seepage velocity, semi-active fine particles (providing lateral support or secondary support for the coarse grains) become susceptible to suffusion if the applied hydraulic stress is high enough to overcome the current effective stress on these particles.

Moreover, some of the particles clogged under a lower seepage velocity are also become prone to erosion under higher hydraulic forces. This is a plausible scenario that explains the behaviour of specimens with the same dimensions but subjected to different seepage velocities (E-D75-V52-T120 and E-D75-V92-T120). **Fig. 3** also shows that even under the maximum seepage velocity (test E-D50-V208-T120), it was not possible to erode all fine particles. This could be because of full contribution of the remaining fine particles (active particles) in the soil skeleton. **Fig. 5** schematically displays erosion progress and particle rearrangement. **Fig. 5 (a)** shows the initial condition of the fine and coarse particles and the stress transferring mechanism. Free fine particles were washed first due to the seepage flow (**Fig. 5 (b)**), semi-active fines started to migrate where locally higher hydraulic gradients were raised due to clogging and released new free fine particles (**Fig. 5 (c)**). Metastable force chains were formed after the erosion of the semi-active fine particles (Mehdizadeh and Disfani, 2018) which led to local coarse particle rearrangements and vertical deformations (**Fig. 5 (d)**).

<<Insert **Fig 5** about here>>

Impact of Erosion on the Global Void Ratio and Particle Size Distribution

The initial global void ratio was calculated using the soil phase relationship. The post-erosion global void ratio was estimated from the total volume of the eroded sample (calculated using deformations from the photogrammetry technique), the mass of eroded particles and the specific gravity. The erosion of fine particles increased the pre-erosion global void ratio of 0.48 to post-erosion values of 0.66, 0.6 and 0.61 for specimens E-D50-V52-T120, E-D75-V52-T120 and E-D100-V52-T120, respectively. The smallest soil specimen (E-D50-V52-T120) showed a higher post-erosion global void ratio although it was subjected to the same seepage

experienced by the two other specimens. This was due to removal of more fine particles for specimen E-D50-V52-T120 during erosion.

Pre and post-erosion particle size distributions (PEPSD) of eroded specimens (E-D50-V52-T120, E-D75-V52-T120 and E-D100-V52-T120) are shown in **Fig. 6**. Specimens with 50 mm diameter were divided into two parts and those with 75 mm and 100 mm diameters were divided into three parts for PEPSD analysis. Top, middle and bottom PEPSDs were similar for E-D75-V52-T120 and E-D100-V52-T120, which also had similar global void ratios and residual fine contents. Regardless of sample dimension, the fine content decreased along the height of the specimens and the top region of the soil specimens lost more fine particles under downward seepage which was found to be in agreement with result of Ke and Takahashi (2012) and Zhong et al. (2018).

<<Insert **Fig 6** about here>>

Impact of Erosion on Vertical Deformation

Vertical strains during the erosion phase were measured at five-minute intervals using the photogrammetry technique (Mehdizadeh et al., 2017a) and are shown in **Fig. 7**. All specimens experienced vertical strain during erosion phase; a sign of erosion of semi-active fines and local breakage of force chains. Interestingly, all specimens experienced a rapid increase in vertical strain at the beginning of seepage when the inflow velocity was very low. Almost all specimens showed step-wise changes in the vertical strain. Although the erosion rate and residual fine content were similar for the 75 and 100 mm specimens (E-D75-V52-T120 and E-D100-V52-T120), the vertical strain was larger in the 100 mm sample. The experiments here and the

analyses based on the method suggested by Kenney et al. (1985) both suggest that the larger the sample is, the higher is the chance of clogging, leading to fewer eroded particles (i.e. those transported by seepage) being washed out of the sample. As fines are more likely to meet a small constriction as the flow paths are longer. However, the pattern of vertical deformation mainly depends on the erosion of semi-active fine particles and the consequent buckling of the force chains. As force chain buckling is caused by local transport of semi-active fines, rather than them being washed out of the sample, there is not necessarily a relationship between fines eroded and vertical strain.

<<Insert **Fig 7** about here>>

Impact of Erosion on Post-erosion Undrained Behaviour

The undrained stress-strain relationship up to 15 percent strain, induced excess pore pressure and stress path of all tested specimens are presented and compared in Fig. 8. To draw a better conclusion, additional erosion tests results for the same initial PSD presented by Mehdizadeh et al. (2017b) (E-D75-V52-T30 and E-D75-V92-T30) on 75 mm diameter samples are also included. Comparing tests result indicates that the post-erosion undrained behaviour of soil specimens regardless of seepage velocity and duration can be divided into three main groups. Specimens E-D75-V52-T30, E-D75-V52-T120 and E-D75-V92-T30 (Fig. 8 (a)) showed similar stress-strain relationship (similar initial peak and ultimate shear strength) and induced excess pore pressures during undrained shearing with different residual fine contents and global void ratios but with the same post-erosion intergranular void ratios ($e_g = \frac{e + FC}{1 - FC}$, e is the global void ratio and FC is the fine content (Mitchell (1993))). The intergranular void ratio was found to be approximately 0.9 for these specimens after erosion. Specimens E-D75-V92-T120, E-

303 D50-V52-T120 and E-D50-V208-T120 (Fig. 8 (b)) had similar post-erosion intergranular void
304 ratios of 0.84-0.86 and showed similar behaviour (similar initial peak and ultimate shear
305 strength). The residual fine content was recorded as 10.1, 10.2 and 6.9 per cent, respectively.
306 The erosion of just an additional 3.3 per cent fine content was observed for specimen E-D50-
307 V208-T120 although it was subjected to a more powerful seepage. This suggests that erosion
308 of the additional fine particles in specimen E-D50-V208-T120 had negligible impact on the
309 post-erosion mechanical behaviour. The undrained behaviour of non-eroded specimens (NE-
310 D75 and NE-D100) was shown in Fig. 8 (d). It is evident that while the hardening behaviour is
311 more dominant in non-eroded specimens compared to all of the eroded specimens especially
312 in higher strains, their initial undrained peak shear strength is lower than eroded specimens
313 regardless of the erosion progress. The excess pore pressure is induced much quicker in the
314 non-eroded specimens and also dropped much faster. The only exception was specimen E-
315 D100-V52-T120 which showed a similar behaviour to specimens E-D75-V52-T30, E-D75-
316 V52-T120 and E-D75-V92-T30 (Fig. 8 (a)) at small strains up to 5% then showed a hardening
317 behaviour like specimens NE-D75 and NE-D100 at large strains. The residual fine content was
318 similar for specimens E-D75-V52-T120 and E-D100-V52-T120, which showed similar trends
319 in small strains (less than five per cent). However, the shear strength increased more rapidly in
320 specimen E-D100-V52-T120 at medium and large strains. This shows that similar post-erosion
321 particle size distribution does not necessarily lead to the same mechanical behaviour, due to
322 sample inhomogeneity and differences in fabric. It is worth noting that the intergranular void
323 ratio suggested by Mitchell (1993) does not consider the level of contribution of fine particles
324 in the soil structure (their erodability potential). Therefore, it is difficult to explain how erosion
325 of fine particles contributes to observed reductions in the intergranular void ratio. However, it
326 seems rearrangement of coarse particles due to loss of semi-active fine particles led to vertical
327 settlement and decrease in intergranular void ratio.

It can be understood from Fig. 8 that with a decrease in the fine content, the softening behaviour became more dominant and the hardening behaviour in large strains decreased. However, all non-eroded and eroded specimens (regardless of sample dimension and rate of erosion) showed an “elbow” in the stress path, which signifies a transition from limited strain softening to a quasi-steady state (initial contraction followed by dilation) (Pitman et al., 1994). In other words, all specimens (eroded and non-eroded) were initially located between the Steady State Line (SSL) and Isotropic Compression Line (ICL) in $e - \log p'$ space as shown by Thevanayagam and Mohan (2000). The mobilized friction angle at initial peak shear stress (ϕ'_{PS}), at the start of dilation (phase transformation, ϕ'_{PT}) and at steady state (ϕ'_{SS}) have been determined for all tested specimens using the axisymmetric principal stress ratio (M) (M is the ratio between q and p' (Table 3). It was found that the mobilized friction angle at the steady state was higher than the mobilized friction angle at initial peak shear stress and at phase transformation state thanks to an increase of dilatancy in large strains regardless of the specimen status in terms of erosion progress and size. It is also evident from Fig. 8 (d, e and f) and Table 3 that all specimens eventually ended up on the same Steady State Line (SSL) as suggested by Yang et al. (2006a) for sand-silt mixtures with various non-plastic fine contents.

<<Insert Fig 8 about here>>

<<Insert Table 3 about here>>

To consider the contribution of active (which can also be considered as non-erodible) fine particles in the soil structure in terms of active grain contacts, Thevanayagam et al. (2002) proposed a density variable called equivalent intergranular contact index ($(e_c)_{eq} = \frac{e + (1-b)FC}{1 - (1-b)FC}$)

when $FC < FC_{th}$, where the critical fine content (FC_{th}) is a fine content above which the coarse particles are no longer in full contact with each other and b is the fraction of active fines. $b=0$ means all fines act exactly like voids and when $b=1$, they are not distinguishable from host sand particles and they actively participate in supporting the soil skeleton. However, the concept of parameter b is controversial. Some researchers (e.g. Thevanayagam et al., 2002; Ni et al., 2004; Yang et al., 2006a, 2006b) believe b is constant for all mixtures with fine contents less than the critical fine content (FC_{th}) and it only depends on grain size disparity ratio ($R_d = D_{50}/d_{50}$) or particle size ratio ($\chi = D_{10}/d_{50}$), where D_{10} particle size of pure sand at 10% finer, D_{50} mean particle size of coarse fraction and d_{50} mean particle size of fine fraction. This means for a specific mixture and regardless of the fine content always percentage of active fine particles is constant. On the contrary, some other researchers (e.g. Rahman et al., 2008; Nguyen et al., 2017) take into account the impact of fine content. However, Chang and Deng (2019) showed that b only depends on D_{50}/d_{50} and effective stress and is independent of fines content for mixtures with small grain size disparity ratio.

The parameter b for the mixture tested in this research can be estimated from the test result on specimen E-D50-V208-T120. Here, it is assumed that all erodible particles were washed out in the sample with 50 mm diameter under the seepage velocity of 208 mm/min (the maximum applicable in the lab) under a two-hour seepage, when it can be seen that erosion rate approached zero (Fig. 3). The applied seepage was unable to erode all fine particles and 6.9 percent was left unwashed at the end of the erosion. By this assumption, 6.9% residual fine content were all non-erodible fine particles and were fully active in the force chains. Therefore, the b parameter is the ratio of active fine particles (6.9%) to total fine particles (25%), i.e. $b = 0.28$. This is in relatively good agreement with calculated b in the range of 0.25-0.4 for the mixtures with the same D_{50}/d_{50} using semi-empirical expressions proposed by Rahman et al.

(2011) and Chang and Deng (2019). b can be estimated for all eroded specimens using their residual fine contents and an assumption that 6.9% of fines are initially active (**Fig. 9 (a)**). Although the amount of active fine particles can be assumed to be constant in all eroded and non-eroded specimens, the parameter b , which is a proportion of the total fine content contributing to load transfer, cannot be constant. Using the calculated b and residual fine content, the equivalent intergranular contact index $(e_c)_{eq}$ can be calculated for each specimen at the beginning of the undrained shearing. Variation of peak shear stress ratio ($\eta_{PS} = \frac{q}{p'}$, where q and p' are deviator and mean effective stresses, respectively) with $(e_c)_{eq}$ for all tested specimens is shown in **Fig. 9 (b)**. The η_{PS} increased initially with a decrease in $(e_c)_{eq}$ (a decrease of the residual fine content down to 15.1 per cent) and then decreased with further reduction in equivalent intergranular contact index (decrease in the residual fine content down to 6.9 per cent). Mehdizadeh et al. (2017a) showed that for the soil mixture used in this research coarse particles were more angular than fine particles. Therefore, the initial improvement in the undrained shear strength (initial peak shear stress, ϕ'_{PS} in **Table 3**) could be due to a better interlock between the coarse particles but without the loss of semi-active fine particles which helps to prevent collapse at small strains. However, further erosion resulted in rearrangement of the coarse particles and loss of semi-active fine particles leading to formation of a metastable structure and a higher tendency to contractive behaviour. It is worth noting that the initial peak shear strength and in particular equivalent intergranular contact index vary over a small range. More experiments are required to validate this finding and establish a relationship between $(e_c)_{eq}$ and fine particles with different levels of contribution in the soil structure, fabric changes and re-deposition of fine particles due to clogging.

<<Insert **Fig 9** about here>>

Conclusion

The influence of internal erosion on soil structure and post-erosion mechanical behaviour of an internally unstable gap-graded soil of different specimen size and flow velocity was examined through laboratory investigation. The following points were the most important findings of this research:

- A step-wise trend was observed in the vertical strains during the erosion phase, which is believed to be due to erosion of semi-active fines that provided lateral support for the force chains.
- Under the same seepage velocity and duration, the erosion of fine particles decreased with an increase in length of specimen, due to higher potential of clogging for eroded particles that travel a longer distance.
- Strain softening behaviour becomes more dominant with a decrease in the residual fine content due to internal erosion.
- The experiments suggested that regardless of dimension of the soil specimens, inflow velocity and seepage duration, specimens with the same post-erosion intergranular void ratios showed similar undrained behaviour. However, more erosion-triaxial tests on samples with different fabrics need to be conducted to draw a clearer conclusion.
- It was found from the experiments in this study that erosion of fine particles up to 15% of the overall sample mass improved the initial undrained peak shear strength. This positive impact later degenerated when a greater percentage of fine particles were lost. However, more validation is required.

- It seems the initial undrained shear strength is affected by equivalent intergranular contact index. However, more experiments are required to validate this finding.
- Suffusion was found to have minimal impact on the steady state line of the mixture studied in this experiment and it seems to be independent of the residual fine content.
- The mixture in this study had coarse and fine particles with different angularities. Erosion of fine particles may change the global interlocking of particles and post-erosion behaviour. Impact of particle shape on erosion and post-erosion behaviour needs further investigation.

References

- Burenkova, V.V. 1993. Assessment of Suffusion in Non- Cohesive and Graded Soils. Proc. 1st Int. Conf. on Geo-Filters, Balkema, Rotterdam, The Netherlands, 357-360.
- Carrier III, W.D. 2003. "Goodbye, Hazen; Hello, Kozeny-Carman," Journal of Geotechnical and Geoenvironmental Engineering, ASCE, **129**(11): 1054-1056.
- Chang, D.S., and Zhang, L.M. 2011. A stress-controlled erosion apparatus for studying internal erosion in soils. Geotechnical testing journal, **34**(6): 579-589.
- Chang, D.S., and Zhang, L.M. 2012. Critical hydraulic gradients of internal erosion under complex stress states. Journal of Geotechnical and Geoenvironmental Engineering, **139**(9): 1454-1467.
- Chang, C.S., and Deng, Y. 2019. Revisiting the concept of inter-granular void ratio in view of particle packing theory. Géotechnique Letters, **9**, 121-129.
- Chen, C., Zhang, L.M., and Chang, D.S. 2016. Stress-Strain Behavior of Granular Soils Subjected to Internal Erosion. Journal of Geotechnical and Geoenvironmental Engineering, 06016014.

- 451 Frost, J.D., and Park, J.Y. 2003. A critical assessment of the moist tamping technique.
452 Geotechnical Testing Journal, **26**(1): 57-70.
- 453 Indraratna, B., Raut, A. K., and Khabbaz, H. 2007. Constriction-based retention criterion for
454 granular filter design. Journal of Geotechnical and Geoenvironmental Engineering,
455 10.1061/(ASCE)1090-0241(2007)133:3(266), 266-276.
- 456 Indraratna, B., Nguyen, V.T., and Rujikiatkamjorn, C. 2011. Assessing the potential of internal
457 erosion and suffusion of granular soils. Journal of Geotechnical and Geoenvironmental
458 Engineering, **137**(5): 550-554.
- 459 International Commission on Large Dams (ICOLD) 2015. Internal erosion of existing dams,
460 levees and dikes, and their foundations. Bulletin 164, Paris.
- 461 Ke, L., and Takahashi, A. 2014. Triaxial erosion test for evaluation of mechanical
462 consequences of internal erosion. Geotechnical Testing Journal, **37**(2): 1-18.
- 463 Ke, L., and Takahashi, A. 2015. Drained Monotonic Responses of Suffusional Cohesionless
464 Soils. Journal of Geotechnical and Geoenvironmental Engineering, **141**(8): 04015033,
465 doi: 10.1061/(ASCE)GT.1943-5606.0001327.
- 466 Kenney, T.C., Chahal, R., Chiu, E., Ofoegbu, G.I., Omenge, G.N., and Ume, C.A. 1985.
467 Controlling constriction sizes of granular filters. Canadian Geotechnical Journal, **22**(1):
468 32-43.
- 469 Kenney, T.C., and Lau, D. 1986. Internal stability of granular filters: Reply. Canadian
470 Geotechnical Journal, **23**(4): 420-423. doi: 10.1139/t86-068.
- 471 Kezdi, A. 1969. Increase of protective capacity of flood control dikes. Department of
472 Geotechnique, Technical University, Budapest. Report No. 1.
- 473 Li, M. 2008. Seepage-induced failure in widely graded cohesionless soils. PhD thesis,
474 University of British Columbia, Vancouver, Canada.

- 475 Locke, M., Indraratna, B., and Adikari, G. 2001. Time-dependent particle transport through
476 granular filters. *Journal of Geotechnical and Geoenvironmental Engineering*, **127**(6):
477 521-529.
- 478 Marot, D., Sail, Y., and Alexis, A. 2010. Experimental bench for study of internal erosion in
479 cohesionless soils. In *Scour and Erosion*, 418-427.
- 480 Marot, D., Bendahmane, F., and Nguyen, H.H. 2012. Influence of angularity of coarse fraction
481 grains on internal erosion process. *La Houille Blanche, International Water Journal*,
482 **6**(2012): 47-53. DOI 10.1051/lhb/2012040.
- 483 Mehdizadeh, A., Disfani, M.M., Evans, R.P., Arulrajah, A. and Ong, D.E.L. 2017a. Mechanical
484 Consequences of Suffusion on Undrained Behaviour of a Gap-graded Cohesionless Soil
485 - An Experimental Approach. *Geotechnical Testing Journal*, **40**(6): DOI:
486 10.1520/GTJ20160145.
- 487 Mehdizadeh, A., Disfani, M.M., Evans, R.P. and Arulrajah, A. 2017b. Progressive Internal
488 Erosion in a gap-graded internally unstable soil-Mechanical and Geometrical Effects.
489 *International Journal of Geomechanics*, **18**(3): 04017160.
- 490 Mehdizadeh, A., and Disfani, M.M. 2018. Micro scale study of internal erosion using 3D X-
491 ray Tomography. The 9th International Conference on Scour and Erosion, Taipei, Taiwan,
492 19-26.
- 493 Mitchell, J.K. 1993. *Fundamentals of soil behavior*. John Wiley & Sons, Inc., New York, N.Y.,
494 1-210.
- 495 Nguyen, T., Benahmed, N., and Hicher, P. 2017. Determination of the equivalent intergranular
496 void ratio – application to the instability and the critical state of silty sand. In *Powders
497 and Grains 2017 – Proceedings of the 8th international conference on micromechanics
498 on granular media*, Montpellier, p. 02019.

- 499 Ni, Q., Tan, T.S., Dasari, G.R., and Hight, D.W. 2004. Contribution of fines to the compressive
500 strength of mixed soils. *Geotechnique*, **54**(9): 561-569.
- 501 Pitman, T.D., Robertson, P.K., and Sego, D.C. 1994. Influence of fines on the collapse of loose
502 sands. *Canadian Geotechnical Journal*, **31**(5): 728-739.
- 503 Rahman, M.M., Lo, S.R., and Gnanendran, C.T. 2008. On equivalent granular void ratio and
504 steady state behaviour of loose sand with fines. *Canadian Geotechnical Journal*, **45**(10):
505 1439-1455.
- 506 Rahman, M.M., Lo, S.R., and Baki, M.A.L. 2011. Equivalent granular state parameter and
507 undrained behaviour of sand-fines mixtures. *Acta Geotechnica*, **6**(4): 183-119,
508 <https://doi.org/10.1007/s11440-011-0145-4>.
- 509 Richards, K. S., and Reddy, K. R. 2008. Experimental investigation of piping potential in
510 earthen structures. *Geotechnical Special Publication*, 178, 367-376.
- 511 Rochim, A., Marot, D., Sibille, L., and Le, V.T. 2017. Effect of hydraulic loading history on
512 the characterization of suffusion susceptibility of cohesionless soils. *Journal of*
513 *Geotechnical and Geoenvironmental Engineering*, **143**(7). DOI
514 10.1061/(ASCE)GT.1943-5606.0001673.
- 515 Seghir, A., Benamar, A., and Wang, H. 2014. Effects of fine particles on the suffusion of
516 cohesionless soils. *Experiments and modelling. Transport in Porous Media*, **103**(2): 233-
517 247.
- 518 Sellmeijer, J.B. 1988. On the mechanism of piping under impervious structures. PhD thesis,
519 Delft University of Technology.
- 520 Shire, T., O'Sullivan, C., Hanley, K. J., and Fannin, R. J. 2014. Fabric and effective stress
521 distribution in internally unstable soils. *Journal of Geotechnical and Geoenvironmental*
522 *Engineering*, 10.1061/(ASCE)GT.1943-5606 .0001184, 04014072.

- 523 Sibille, L., Marot, D., and Sail, Y. 2015. A description of internal erosion by suffusion and
524 induced settlements on cohesionless granular matter. *Acta Geotechnica*, **10**(6): 735-748.
- 525 Taylor, H.F., O'Sullivan, C., Shire, T., and Moinet, W.W. 2019. Influence of the coefficient of
526 uniformity on the size and frequency of constrictions in sand filters. *Géotechnique*, **69**(3):
527 274-282.
- 528 Thevanayagam, S., and Mohan, S. 2000. Intergranular state variables and stress-strain
529 behaviour of silty sands. *Geotechnique*, **50**(1): 1-23.
- 530 Thevanayagam, S., Shenthana, T., Mohan, S. and Liang, J. (2002). Undrained fragility of clean
531 sands, silty sands, and sandy silts. *Journal of Geotechnical and Geoenvironmental*
532 *Engineering*, 128(10): 849-859, [https://doi.org/10.1061/\(ASCE\)1090-0241](https://doi.org/10.1061/(ASCE)1090-0241(2002)128:10(849))
533 (2002)128:10(849).
- 534 Vogt, N., Simpson, B., Van Seters, A., Gens, A., Odenwald, B., Moller, H., Habert, J., and
535 Panu, T. 2015. TC250/SC7/EG9: Water pressures. Final Report: Proposal of changes to
536 EC7-1.
- 537 Wu, L., Nzouapet, B.N., Vincens, E., and Bernat-Minana, S. 2012. Laboratory experiments for
538 the determination of the Constriction Size Distribution of granular filters. In *Proceedings*
539 *of the 6th international conference on scour and erosion, ICSE-6*, pp. 233-240. Paris,
540 France: SHF.
- 541 Xiao, M., and Shwiyhat, N. 2012. Experimental investigation of the effects of suffusion on
542 physical and geomechanic characteristics of sandy soils. *Geotechnical Testing Journal*,
543 **35**(6): 890-900.
- 544 Yang, S. L., Sandven, R., and Grande, L. 2006a. Steady-state lines of sand-silt
545 mixtures. *Canadian Geotechnical Journal*, **43**(11): 1213-1219.

- 546 Yang, S.L., Sandven, R., and Grande, L. 2006b. Instability of sand-silt mixtures. *Soil Dynamic*
547 *and Earthquake Engineering*, **26**(2–4): 183-190,
548 <https://doi.org/10.1016/j.soildyn.2004.11.027>.
- 549 Zhong, C., Le, V.T., Bendahmane, F., Marot, D., and Yin, Z.Y. 2018. Investigation of spatial
550 scale effects on suffusion susceptibility. *Journal of Geotechnical and Geoenvironmental*
551 *Engineering*, **144**(9): 04018067. DOI: 10.1061/(ASCE)GT.1943-5606.0001935.
- 552

Draft

553 **Figure Captions:**

554 Fig 1. Particle size distribution of the tested soil sample (After Mehdizadeh et al., 2017a)

555 Fig 2. Variation of inflow velocity with time

556 Fig 3. Variation of normalized residual fine content with time

557 Fig 4. Effective Constriction Size Distribution (CSD) at different heights in the sample
558 according to the method suggested by Kenney et al (1985)

559 Fig 5. Progress of internal erosion (a) Initial condition, (b) Erosion of the free fines, (c) Erosion
560 of the semi-active fines and providing new free fines and (d) Particles rearrangement and
561 vertical deformation with residual active fines

562 Fig 6. Particle size distribution plots for post-erosion specimens at different regions for (a) E-
563 D50-V52-T120, (b) E-D75-V52-T120 and (c) E-D100-V52-T120

564 Fig 7. Vertical strains during erosion phase

565 Fig 8. Impact of internal erosion on undrained stress-strain relationship, induced excess pore
566 pressure and stress path of eroded and non-eroded specimens during undrained shearing

567 Fig 9. (a) Variation of the parameter b with residual fine content and (b) Variation of peak
568 shear stress ratio with equivalent intergranular contact index

569 **Table Captions:**

570 Table 1. Physical properties of tested soil sample (After Mehdizadeh et al., 2017a)

571 Table 2. Erosion-triaxial testing program

572 Table 3. Mobilized friction Angle

Draft

Table 1. Physical properties of tested soil sample (After Mehdizadeh et al., 2017a)

Physical property	Value	Physical property	Value
Maximum void ratio, e_{max}	0.67	D^* , (mm) ^a	0.28 - 0.3
Minimum void ratio, e_{min}	0.36	Initial Void Ratio, e_i	0.48
Initial Moisture Content, MC (%)	6	Relative Density, D_r (%)	60
Uniformity coefficient, C_u	12.14	$(D'_{15}/d'_{85})^b$	5.2
Gap ratio, G_r	3.93	$(H/F)_{min}^c$	0.08

^a: Controlling constriction size (Kenney et al., 1985 and Indraratna et al., 2007)

^b: D'_{15} is the particle diameter in which 15 per cent by weight of coarser particles passed and d'_{85} is the particle diameter in which 85 per cent by weight of fine particles passed. Soils with $(D'_{15}/d'_{85}) > 4$ are considered internally unstable (Kozdi, 1969).

^c: F is the passed fraction by weight finer than d , and H is the weight fraction between d and $4d$ (Kenney and Lau 1985, 1986).

Draft

Table 2. Erosion-triaxial testing program

Test Series	Sample Label	Sample Diameter (mm)	Sample Height (mm)	Seepage Velocity (mm/min)	Hydraulic Gradient ^a	Erosion Duration (min)	CIU ^b Test
1	E-D50-V52-T120 ^c	50	115 ^d	52	1.15	120	Yes
	E-D75-V52-T120 ^c	75	150	52	1.15	120	Yes
	E-D100-V52-T120	100	200	52	1.15	120	Yes
2	E-D75-V92-T120 ^c	75	150	92	2.04	120	Yes
3	E-D50-V208-T120	50	115	208	4.6	120	Yes
4	NE-75 ^f	75	150	-	-	-	Yes
	NE-100	100	200	-	-	-	Yes

^a: assuming Darcy's Law and having initial hydraulic conductivity of 0.075 cm/s

^b: Isotropically Consolidated Undrained Triaxial Test

^c: E-D50-V52-T120 means E (Eroded)-D (Diameter (mm))-V (Seepage velocity (mm/min))-T (Seepage duration (min))

^d: This sample had a height to diameter ratio of 2.3 which was higher than other specimens. It was attributed to the height of the mould.

^e: Reported by Mehdizadeh et al. (2017b)

^f: NE-50 means NE (Non-Eroded)-D (Diameter) and reported by Mehdizadeh et al. (2017a)

Draft

Table 3. Mobilized friction Angle

Specimen	FC_f (%)	ϕ'_{PS} (°)	ϕ'_{PT} (°)	ϕ'_{SS} (°)
E-D75-V52-T30	19.8	27	30	32
E-D75-V52-T120	15.9	27	29	32
E-D75-V92-T30	18.6	27	30	32
E-D100-V52-T120	15.1	30	30	32
E-D50-V52-T120	10.2	25	29	32
E-D50-V208-T120	6.9	24	29	32
E-D75-V92-T120	10.1	27	30	32
NE-75	25	26	30	32
NE-100	25	25	27	32

Draft

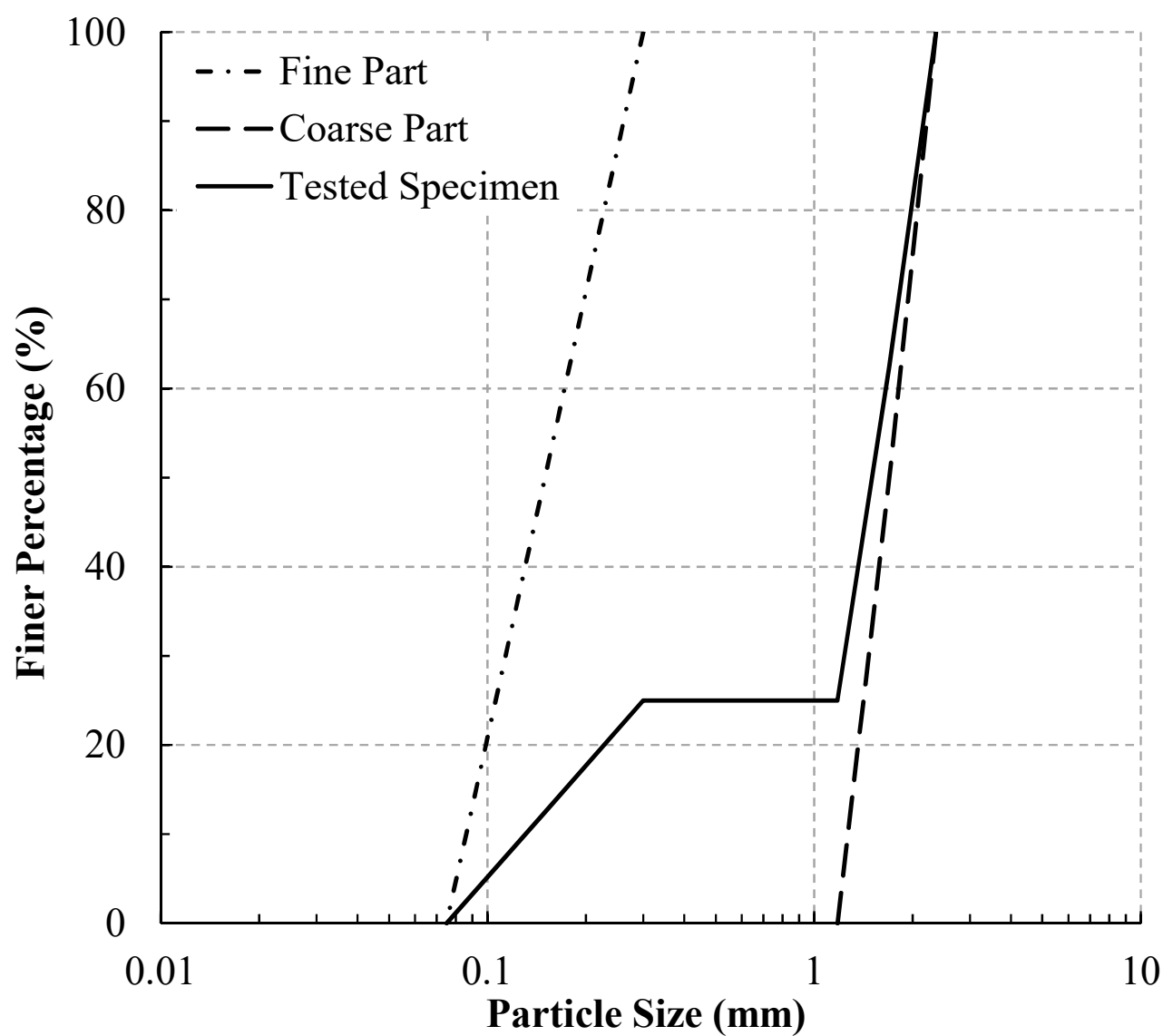


Fig 1. Particle size distribution of the tested soil sample (After Mehdizadeh et al., 2017a)

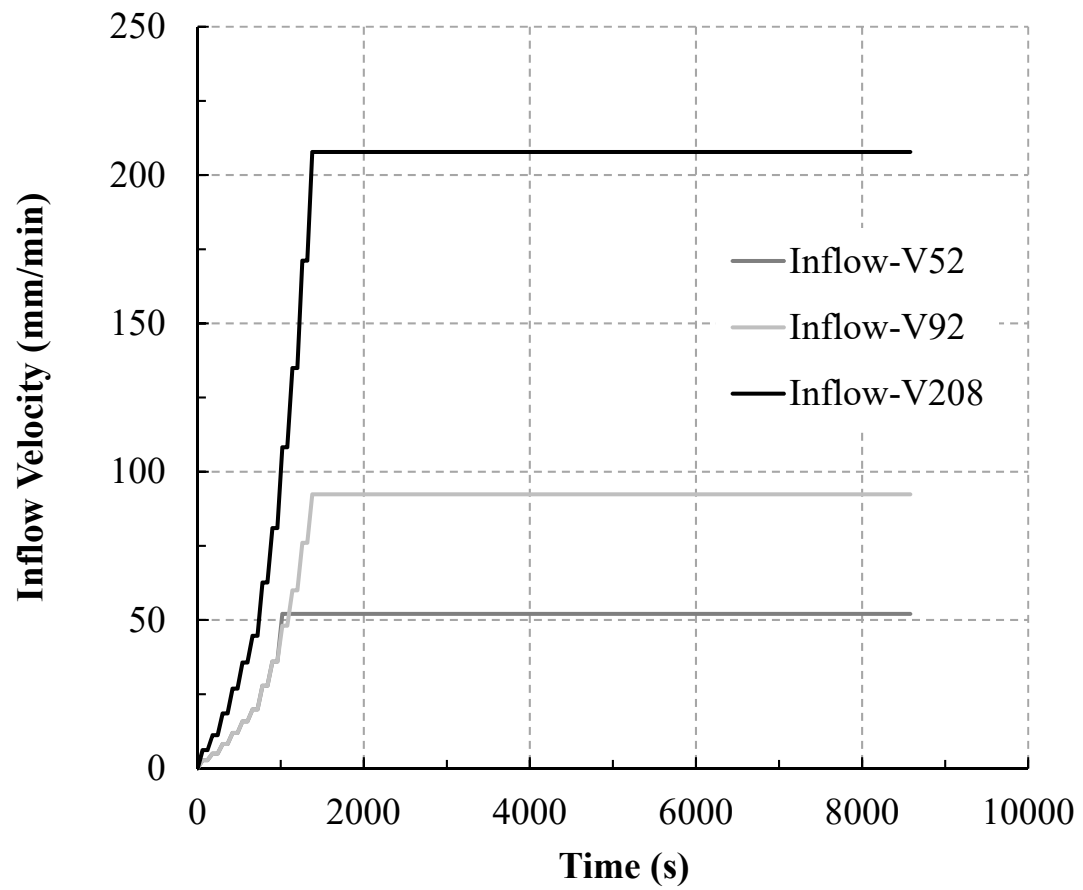


Fig 2. Variation of inflow velocity with time

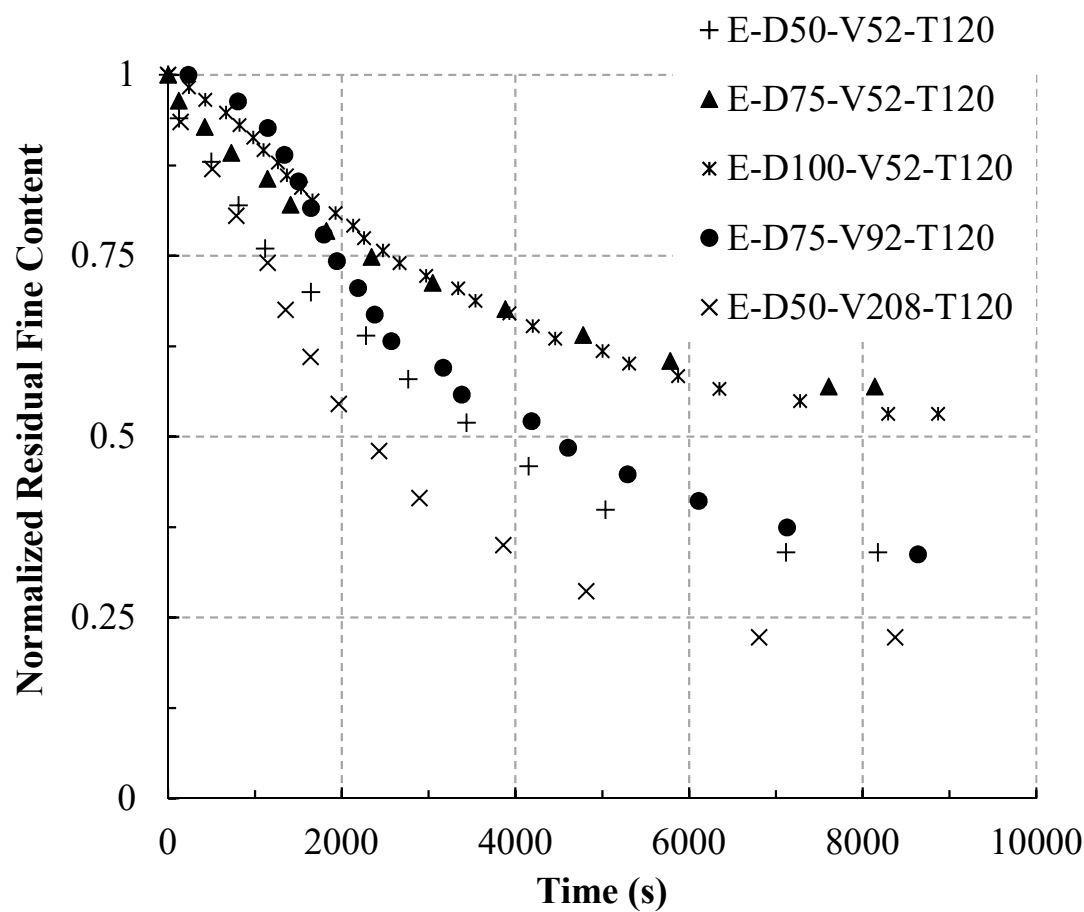


Fig 3. Variation of normalized residual fine content with time

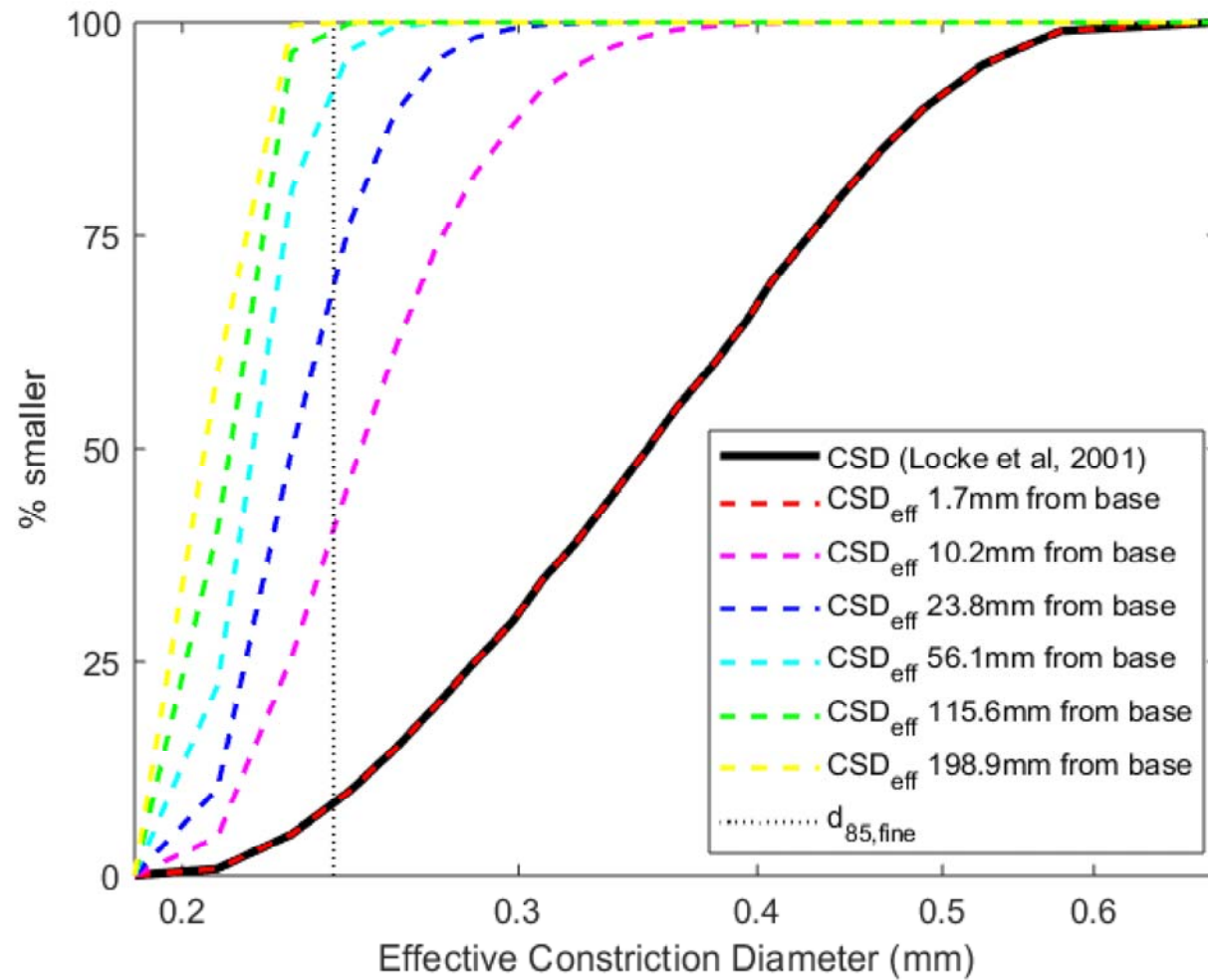


Fig 4. Effective Constriction Size Distribution (CSD) at different heights in the sample according to the method suggested by Kenney et al (1985)

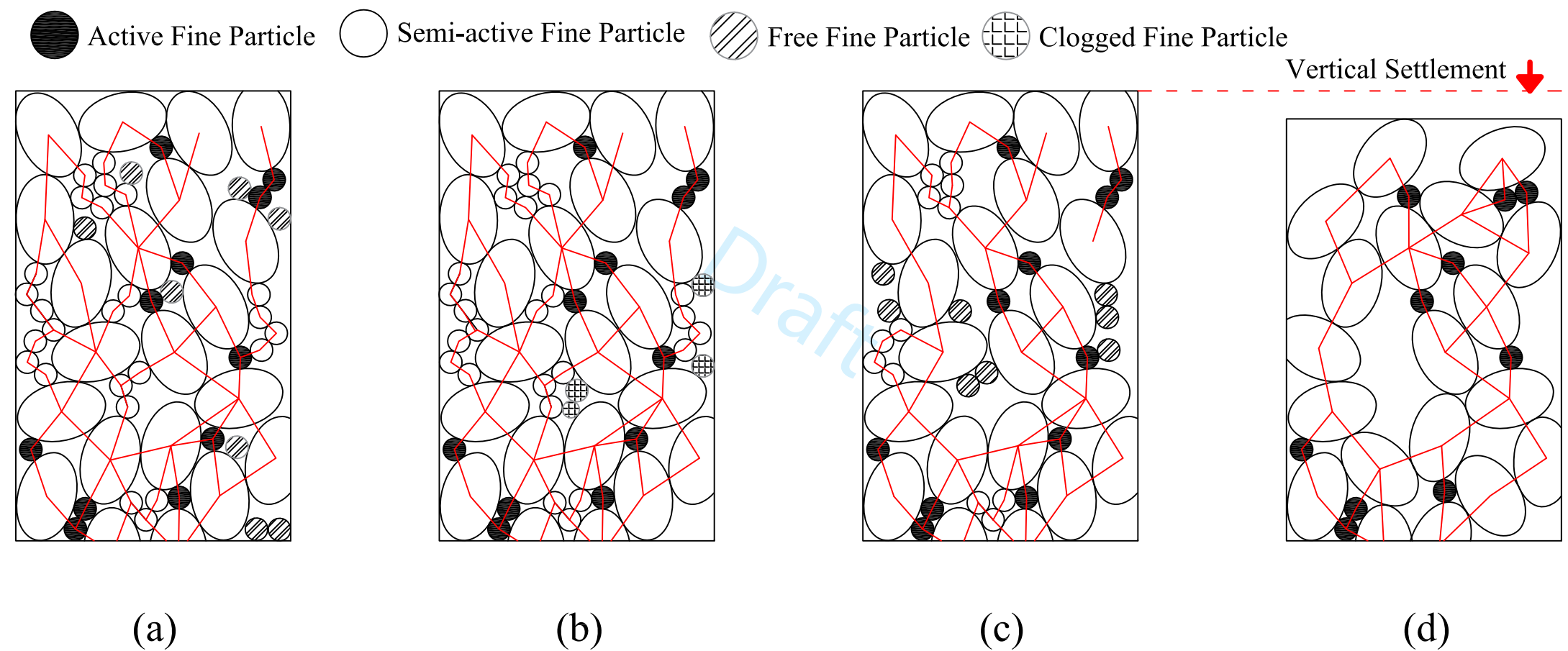


Fig 5. Progress of internal erosion (a) Initial condition, (b) Erosion of the free fines, (c) Erosion of the semi-active fines and providing new free fines and (d) Particles rearrangement and vertical deformation with residual active fines

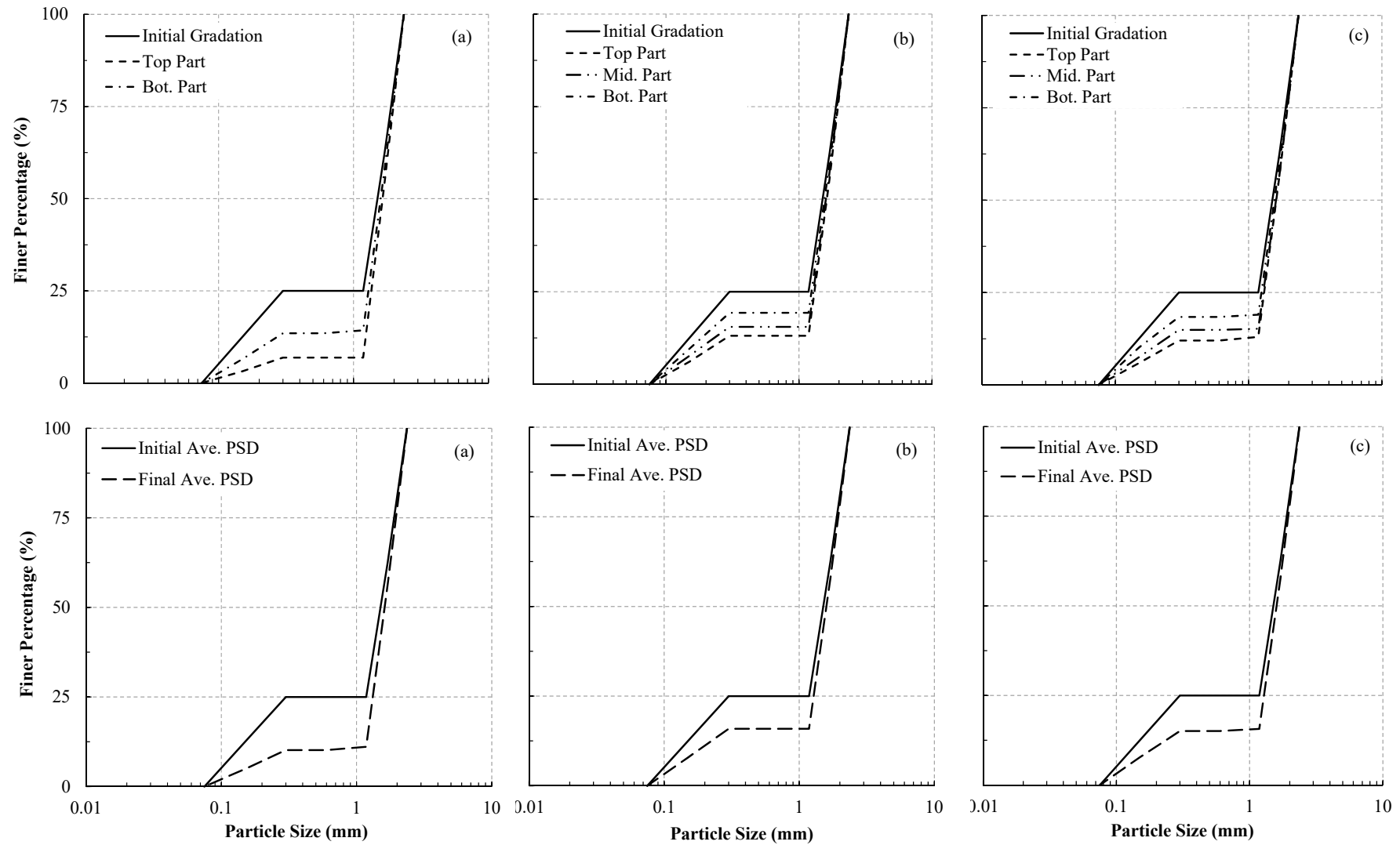


Fig 6. Particle size distribution plots for post-erosion specimens at different regions for (a) E-D50-V52-T120, (b) E-D75-V52-T120 and (c) E-D100-V52-T120

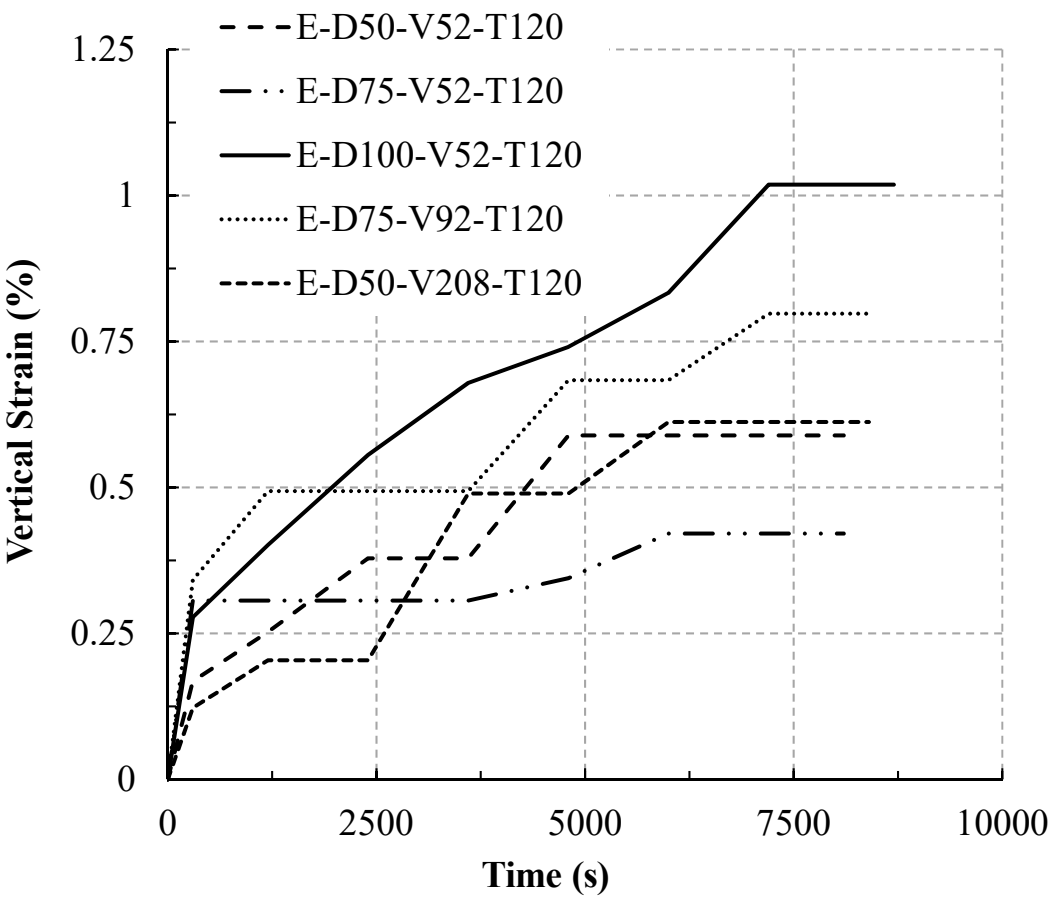


Fig 7. Vertical strains during erosion phase

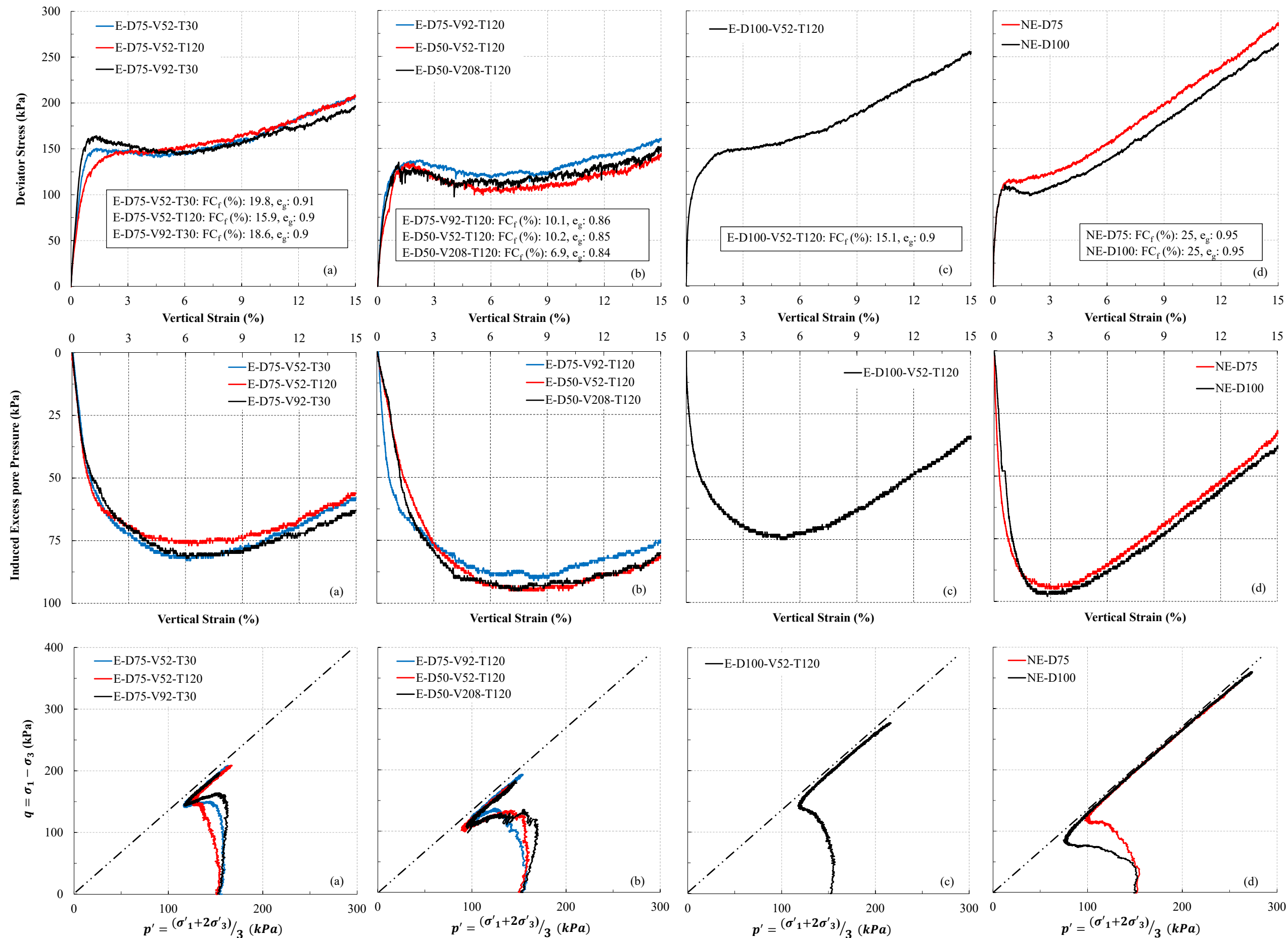


Fig 8. Impact of internal erosion on undrained stress-strain relationship, induced excess pore pressure and stress path of eroded and non-eroded specimens during undrained shearing

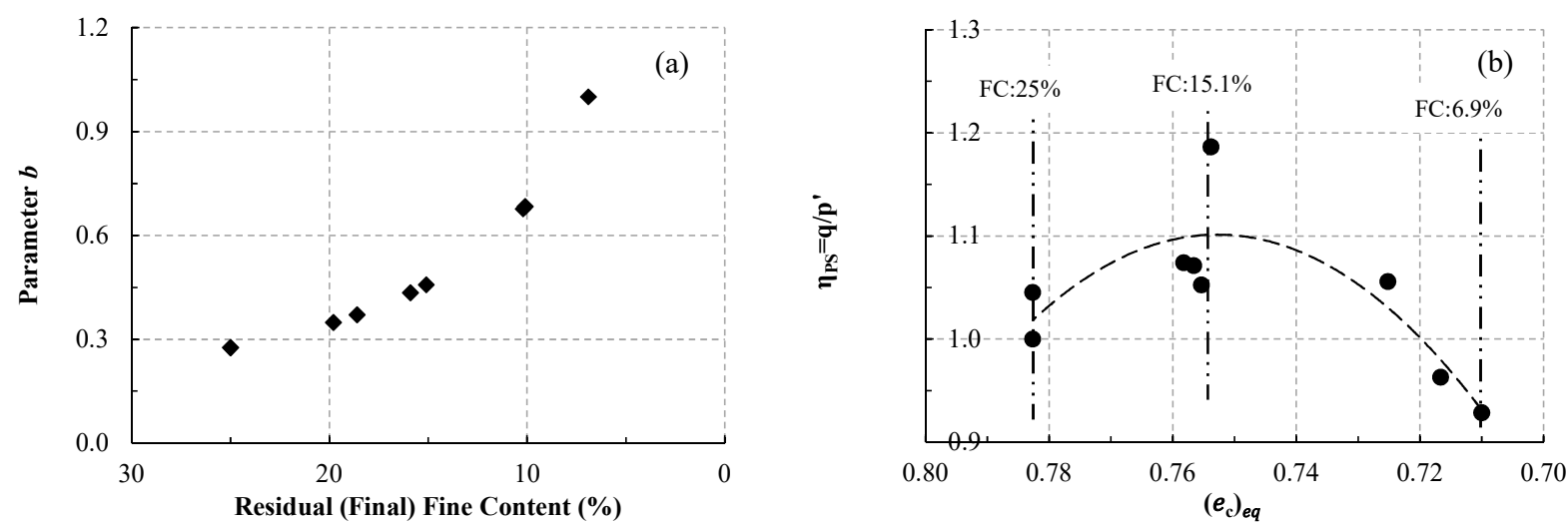


Fig 9. (a) Variation of the parameter b with residual fine content and (b) Variation of peak shear stress ratio with equivalent intergranular contact index